The influence of a slope break on turbidite deposits

An experimental investigation

Pohl, F.; Eggenhuisen, J.T.; Cartigny, M.J.B.; Tilston, M.G.; de Leeuw, J.; Hermidas, N.

Important note
To cite this publication, please use the final published version (if applicable).
Please check the document version above.
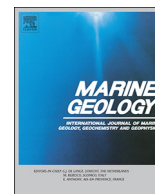
The influence of a slope break on turbidite deposits: An experimental investigation

F. Pohl[a,b,*], J.T. Eggenhuisen[a], M.J.B. Cartigny[c], M.C. Tilston[a], J. de Leeuw[a], N. Hermidas[d]

[a] Faculty of Geosciences, Utrecht University, P.O. Box 80021, 3508 TA Utrecht, the Netherlands
[b] Department of Earth Science, Durham University, Lower Mountjoy South Road, DH1 3LE Durham, UK
[c] Department of Geography, Durham University, Lower Mountjoy South Road, DH1 3LE Durham, UK
[d] Faculty of Civil Engineering and Geosciences, TU Delft, P.O. Box 5048, 2600 GA Delft, the Netherlands

ABSTRACT

Bypassing turbidity currents can travel downslope without depositing any of their suspended sediment load. Along the way, they may encounter a slope break (i.e. an abrupt decrease in slope angle) that initiates sediment deposition. Depending on the initiation point of deposition (the upslope pinch-out), these turbidite deposits in slope-break systems can form potential reservoirs for hydrocarbons. Here we investigate the distribution of turbidite deposits as a function of the geometry of slope-break systems in flume experiments. Shields-scaled turbidity currents were released into a flume tank containing an upper and a lower slope reach separated by a slope break. These slope-break experiments were generating both depositional and bypassing flows solely based on variation in steepness of the lower and upper slope. Results show that the depositional pattern in a slope-break system is controlled by the steepness of the upper and lower slope, rather than the angle of the slope break. The steepness of the upper slope controls the upslope pinch-out, while the lower slope controls the deposit thickness downstream of the slope break.

1. Introduction

Turbidity currents are subaqueous currents of sediment-laden water that move downslope as the result of the density difference between the flow and the surrounding ambient water. They represent a principal mechanism for transporting sediment into the deep ocean (e.g. Mutti et al., 2009; Talling et al., 2015). Multiple turbidity current events can produce submarine channels, which allow the currents to bypass their sediment down the continental slope onto the deep-marine abyssal plain (Daly, 1936; Maier et al., 2011; Stevenson et al., 2015). Following Stevenson et al. (2015), we refer to a bypassing turbidity current as a flow that keeps its entire sediment load in suspension or traction, thereby preventing any deposition. Along their downflow trajectory, turbidity currents may encounter a slope break, marked by a decrease in the ocean-floor gradient. Slope breaks tend to occur in ponded basins, on stepped slopes (Amy, 2019; Brooks et al., 2018; Jobe et al., 2017; Prather, 2003; Prather et al., 2012a, 2012b), and at the base of steep active continental margins (Bourget et al. 2011; Lee et al. 2002). On the more gently dipping ocean floor downstream of the slope break, turbidity currents usually switch from bypassing to depositional conditions, thereby forming sediment bodies (e.g. Amy et al. 2000; Hansen

et al. 2019; Mutti and Normark, 1987, 1991; Prélat et al. 2010).

Sandy deposits in slope-break systems can serve as potential reservoirs for hydrocarbons if these hydrocarbons are trapped (Amy 2019; Hansen et al. 2019; Pettingill 2004; Weimer and Slatt 2004; Zou et al. 2015). Common trapping mechanisms are: (1) structural trapping by post depositional faulting and displacement of reservoirs sands, (2) stratigraphic trapping by sediment bypass and erosion during – or shortly after – deposition of the reservoir sands, or (3) a combination of structural and stratigraphic trapping (Amy 2019 and references therein). In proximal basin locations, the most common inferred trapping mechanisms are sediment bypass and erosion, thus forming a stratigraphic pinch-out trap (Amy 2019). Well-known examples of up-slope stratigraphic pinch-out traps are the Buzzard Field in the Central North Sea, and the Foinaven Field western of the Shetland's (Amy 2019; Doré and Robbins 2005; Ray et al. 2010; Straccia and Prather 1999). In a slope-break setting, the upslope location of the stratigraphic pinch-out trap is crucial for the development of a sealed reservoir. If the upslope pinch-out is located upstream of the slope break, the basin floor sediments are connected to slope sediments, also called thief sands, creating upslope-migration pathways for hydrocarbons (e.g. Amy 2019; Hansen et al. 2019). In contrast, an upslope pinch-out located downstream of

---

the slope break will result in basin-floor sediments that are detached from the slope sediments, forming a stratigraphic pinch-out trap and making upslope leakage of hydrocarbons unlikely. Hence, the location of the upslope stratigraphic pinch-out is of major interest for the recognition and development of reservoirs in slope-break systems.

We present flume tank experiments to investigate the impact of the slope-break geometry on the location of the upslope pinch-out, and the thickness distribution of the resulting deposits. Numerous experiments have studied turbidity currents in slope-break settings (Garcia and Parker 1989; Garcia, 1993, 1994; Gray et al., 2005, 2006; Islam and Imran 2010; Marr et al. 2001; Mulder and Alexander 2001; Toniolo et al. 2006), often associated with rapid transformation of the current dynamics over the slope break, such as hydraulic jumps (Garcia and Parker 1989; Garcia, 1993, 1994; Islam and Imran 2010) or a marked increase in turbulent kinetic energy (Gray et al., 2005, 2006). However, all of the above-mentioned studies used continuously depletive currents (sensu Kneller and Branney 1995), where deposition was initiated immediately after entering the experimental setup, even when the initial slope was steep. In such depletive conditions there is no upslope pinch-out as the deposits are continuous throughout the flume (e.g. Garcia and Parker 1989; Garcia 1994). As a consequence, the impact of the slope break on deposition was commonly rather unclear, and could only be evaluated on the basis of small variations in the thickness of the deposits (Gray et al., 2005, 2006; Mulder and Alexander 2001). For the present experiments, we used Shields scaling of sediment mobility (e.g. de Leeuw et al. 2016; Fernandes et al. 2019), to generate turbidity currents that are able to bypass on the steepest of our experimental slopes, and transform to depositional currents on more gentle slopes. Furthermore, most previous slope-break studies used fixed horizontal, or slightly dipping basin floors down-dip of the slope break (Garcia and Parker 1989; Garcia, 1993, 1994; Gray et al., 2005, 2006; Islam and Imran 2010; Marr et al. 2001; Mulder and Alexander 2001; Toniolo et al. 2006). While this condition may represent the condition for lobes on very gently dipping surfaces, it neglects systems with steeper basin floors (e.g. stepped slopes). Instead, in the set-up used in the experiments presented here both the lower slope and upper slope could be adjusted independently. This allowed us to investigate the effect of basin-floor slope on the depositional pattern independently.

In total, 45 combinations of different upper and lower slope conditions were tested. The results allow us to answer two prominent research questions: (1) How does the gradient before and after the slope break affect the location of the upslope pinch-out? (2) How is the deposit thickness controlled by the gradients before and after the slope break?

2. Methods

2.1. Scaling

Many studies have applied Froude scaling of flow processes, which maintains similarity in the ratio of kinematic to potential energy of the flow by setting a similar Froude number, and ensures turbulent flow with a sufficiently high Reynolds number. The focus of additional Shields scaling in this study is to ensure that physical processes of sediment erosion, transport, and deposition occur in a similar regime as in natural turbidity currents. Shields scaling achieves similarity of the sediment transport regime by setting the particle Reynolds number (Re_p) and aiming for similarity of the Shields parameter (Θ). The Shields-scaling approach has been discussed in previous studies for sediment transport in rivers and shallow seas (e.g. Hughes 1993; Peakall et al. 1996; Yalin 1971), and it has recently been applied in experimental turbidity current studies (de Leeuw et al., 2016, 2018a, 2018b; Eggenhuisen et al. 2019; Ferguson et al. 2020; Fernandes et al. 2019; Miramontes et al. 2020; Pohl et al., 2019, 2020). Given the significance of this approach for turbidity current studies, the following provides a detailed procedure on the application of Shields scaling.

Shields scaling of turbidity currents necessitate a priori evaluation of the general flow and sediment characteristics in nature and the laboratory. The aim of this evaluation is to organize the boundary conditions of the experiments in such a way that the developing turbidity currents are broadly dynamically similar to a natural turbidity current. The initial objective is thus not to calculate precise values of the flow properties, which is also not possible because these properties are only broadly known for natural systems.

The particle Reynolds number is defined as:

$$Re_p = \frac{u_* d}{\nu},\tag{1}$$

where u_* is the shear velocity (m/s), d the grain size of the sediment (m), and ν the kinematic viscosity ($1.3 * 10^{-6}$ m^2/s at 10 °C). Measurements on natural turbidity currents in submarine canyons revealed Re_p of 2–20 (Azpiroz-Zabala et al. 2017; Fernandes et al. 2019). Previous work using our experiment setup has reported shear velocities of ~0.07 m/s (Cartigny et al. 2013). Knowing this, the Re_p can be altered by manipulating d, which was set to a fine grain size ($d_{10} = 35$ μm, $d_{50} = 133$ μm, $d_{90} = 214$ μm; Supplementary material Fig. S1) to achieve Re_p values of ~7, which is centrally placed within the natural range of 2–20. It is noted that the kinematic viscosity increases significantly with the sediment concentration (e.g. Boyer et al. 2011), but this effect occurs equally in laboratory experiments and in the high-density basal layer of real world turbidity currents (Paull et al. 2018).

The Shields parameter θ is the ratio between the fluid shear stress and the gravity force acting on sediment particles (Shields 1936):

$$\theta = \frac{\rho_t u_*^2}{(\rho_s - \rho_w)gd},\tag{2}$$

where ρ_s is the density of the suspended sediment (2650 kg/m^3), ρ_w is the density of water (1000 kg/m^3), and g the gravitational acceleration (9.81 m/s^2). The density of the turbidity current ρ_t is:

$$\rho_t = \rho_s \cdot C + \rho_w (1 - C),\tag{3}$$

with C as the sediment concentration. The shear velocity u_* is used to describe the turbulent shear at the base of the flow and is related to the bed shear stress. The shear velocity is a key variable in the evaluation of the sediment transport capability of a flow (Eggenhuisen et al. 2017; Rouse 1937). Here the shear velocity is estimated by assuming a logarithmic velocity profile between the bed and the velocity maximum u_m (Cartigny et al. 2013; Middleton and Southard 1984; van Rijn 1993):

$$u_* = U_m \kappa \left(\ln\left(\frac{h_m}{0.1 d_{90}} \right) \right)^{-1},\tag{4}$$

κ is the von Kármán constant with 0.4. The thickness of the flow to the height of the velocity maximum is h_m.

Studies on natural flows report θ –values of 0.2–10 (Azpiroz-Zabala et al. 2017; de Leeuw et al. 2016; Fernandes et al. 2019). To meet these values in the experiments, the sediment concentration, the slope gradient, and the grain size of the suspended sediment were adjusted. We required turbidity currents with a flow thickness of ~0.1 m, flowing on slopes in between 2 and 12°, in order to be able to generate a variety of different slope-break system geometries in the available flume. The grain size of the suspended sediment was already determined by the particle Reynolds number at $d_{50} = 133$ μm. Therefore, we set the initial sediment concentration C for the modeled turbidity currents at 17% vol to meet the required θ –values of 0.2–10. With this sediment concentration the modeled flows can be described as high-density turbidity currents (Kuenen and Migliorini 1950; Cartigny et al. 2013). Recent seafloor measurements from full-scale turbidity currents suggest high basal sediment concentrations are common in natural systems (i.e. > 10% vol; Paull et al. 2018). The similarity in sediment concentrations make it likely that sediment exchange between the

Fig. 1. Sketch of the experiment setup. The dip angle of the upper slope was varied from 0 to 12° and the angle of the lower slope from 0 to 8° (both angles with respect to the horizontal). Inset view shows the separation of the flume tank into two channels; one was used for the turbidity current, while the second provides space for the backflow. UVP: Ultrasonic Velocimetry Probe.

sediment bed and the high-density flow is governed by the same processes that include grain-to-grain interactions, and hindered settling (Heerema et al. 2020).

Froude numbers are also calculated to qualify the flow criticality of the turbidity currents. Depth-average densimetric Froude numbers (*Fr′*) were estimated using:

$$Fr' = \frac{U}{\sqrt{g'h}}, \tag{5}$$

The thickness of the flow *h* is here defined as the height at which the velocity *u* is half the velocity maximum U_m (Buckee et al. 2001; Gray et al. 2005; Launder and Rodi 1983). *U* is the depth-averaged velocity and *g′* is submerged gravity defined as:

$$g' = g \frac{(\rho_t - \rho_w)}{\rho_t}, \tag{6}$$

2.2. Flume tank setup and experimental procedure

Experiments were conducted in a flume tank 4 m × 0.5 m × 0.2 m (length x height x width) with a variable slope break (Fig. 1). The turbidity currents left the flume through a free over-fall into an expansion tank (3 m × 2 m × 1.8 m, with a floor 0.3 m lower than the flume tank floor). The currents could expand freely in the expansion tank and produced a weak reflection wave that was too slow to travel back into the experimental setup during the experiment. The flume and expansion tank were filled with fresh water. Sediment with an identical grain size to the sediment used in the turbidity currents was glued to the flume floor to create a rough, non-erodible substrate. A longitudinally oriented separation wall subdivided the flume tank into two, 0.1 m wide channels (see inset view in Fig. 1) to minimize the effect of backflow from the expansion tank into the flume during the experiments. Backflow is generated in flumes to balance the water entrained into the top of the turbidity currents. The severity of the effect of this backflow is reduced by providing additional space on the other side of the separation wall for the water flowing back from the expansion tank into the flume. A cantilevered false-floor was installed to adjust the bed slopes on the upper and lower slope segments (Fig. 1). The steepness of the upper slope was varied between 2 and 12°, and the steepness of the lower slope between 0 and 8° (both angles relative to the horizontal). This resulted in 10 unique slope-break angles and 45 unique combinations of the upper and lower slope conditions (Fig. 2).

A mixture of sediment and fresh water with a volume of 0.45 m³ was prepared in a mixing tank. The grain size of the sediment was measured with a laser particle sizer (Malvern Mastersizer 2000;

Fig. 2. Slope-break systems which were used in this study. A total of 45 different combinations of upper and lower slope angles were tested. The angles of the lower and upper slope are relative to the horizontal. The slope break is the angle between the upper and the lower slope.

Supplementary material Fig. S1). The density of the sediment was 2650 kg/m³. The sediment concentration in the mixture was set to 17% vol as prescribed by the Shields scaling, which is equivalent to a bulk density of 1280 kg/m³, for each experiment. The mixture was pumped into the flume tank through a 4 m long pipe (diameter = 0.06 m) with a radial-flow pump and monitored by a discharge meter (Krohne Optiflux 2300). The discharge was set to 12.5 ± 0.7 m³/h, resulting in a mean flow velocity of 0.81 ± 0.04 m/s at the inlet box. The discharged was held at a constant level by computer-controlled adjustment of the pump speed. The duration of an experiment was ca. 100 s. Video analysis showed that the end of all experimental currents were accompanied by the deposition of a 7–10 mm thick layer of sediment over the entire length of the flume, which is hereafter called the waning-phase deposit. The waning phase deposits were deposited in all experiments, as the result of the rapid decrease of discharge at the end of experiments and the subsequent collapse of the flow (sensu Kneller and Branney 1995) that caused the rapid deposition of all suspended sediment. This process occurred even in experiments with steep slopes, were the steady body of the flow was bypassing. The waning phase deposits do not represent the depositional pattern of the steady body of the flow and were neglected in further analysis.

2.3. Acquisition of the depositional pattern

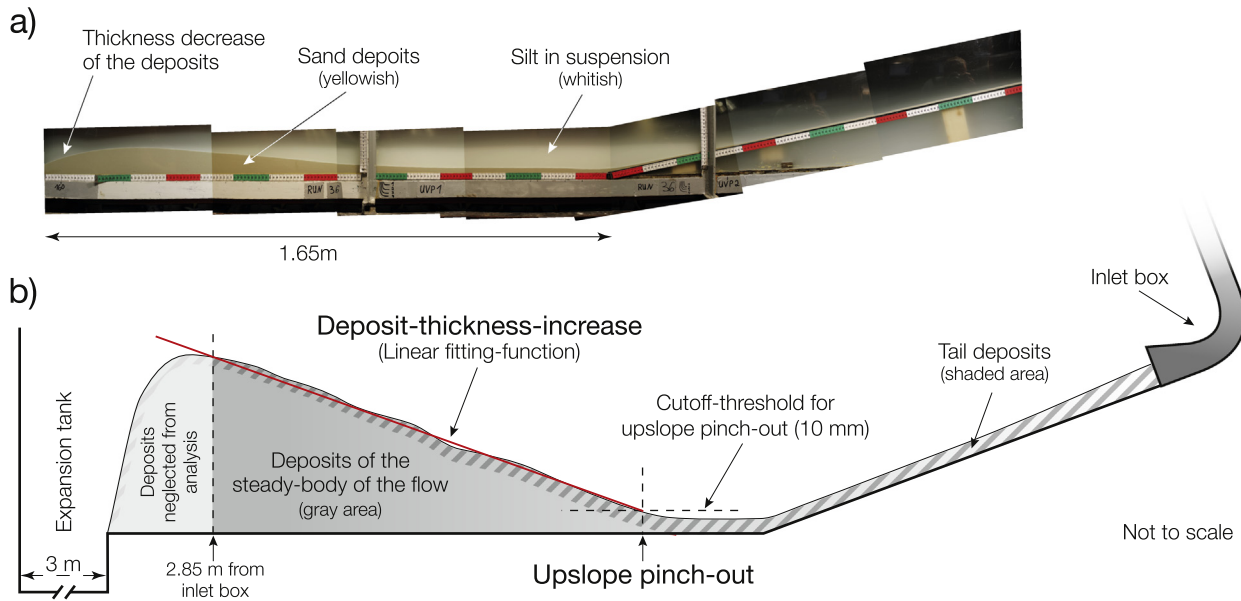The thickness of the deposits was manually measured through the

Fig. 3. (a) Photograph of the deposits of taken shortly after the end of an experiment. At the time the picture was taken, the silt fraction of the sediment was still in suspension. (b) Sketch illustrating the methods applied to analyze and parameterize the deposit profiles.

glass side-wall at longitudinal intervals of 0.05 m prior to draining the flume. Visual inspection through the side glass wall revealed that the thickness of the deposits was constant over the width of the 10 cm wide channel. In all non-bypassing runs, deposit thickness decreased abruptly over the final ~0.35 m of the flume (Fig. 3a). This abrupt thinning of the deposit was an artifact of the transition from the flume into the expansion tank. Consequently, the last 0.5 m of the depositional profiles are omitted from the analysis (Fig. 3b).

The upslope pinch-out is defined as the point where deposit thickness initially exceeded 10 mm. The value of 10 mm was chosen to disregard the waning phase deposits (cf. Fig. 3b) therefore the origins of the upslope pinch-out are associated with the head and body of the currents. Downstream of the upslope pinch-out the thickness of the deposits increased (Fig. 3b). The rate of thickness increase is here referred to as the deposit-thickness-increase. The deposit-thickness-increase was calculated by taking the slope of a local linear regression that was applied to the depositional profile. The range of the fitting function was from the upslope pinch-out to 2.85 m downstream of the inlet box (Fig. 3b).

2.4. Flow dynamic measurements

The flow velocity and density were measured in a reference-experiment as a check of the correct scaling conditions. The reference-experiment was conducted on a 6° dipping flume-tank floor with no slope break. This condition was chosen because it represents an intermediate case within our dataset (Fig. 2).

Flow velocity was measured with an Ultrasonic Velocimetry Profiler (UVP) 2.3 m downstream of the inlet. The UVP probe was positioned 0.11 m above the bed, angled 60° relative to the local bed slope (Figs. 1 and 4a). UVP data acquisition settings are provided in Supplementary material Table S1. The UVP measures velocities of the suspended particles along the beam-axis, and this is converted into a bed-parallel component with the assumption that the bed-normal component is ~0 m/s (Fig. 4a). This assumption was verified in a test experiment with a vertically-oriented UVP. Measured bed-normal velocities were < 0.02 m/s, which is only a fraction (~2%) of the downstream velocity component.

A time-averaged velocity profile was calculated for the body of the current, which is associated with steady-flow conditions. The start of
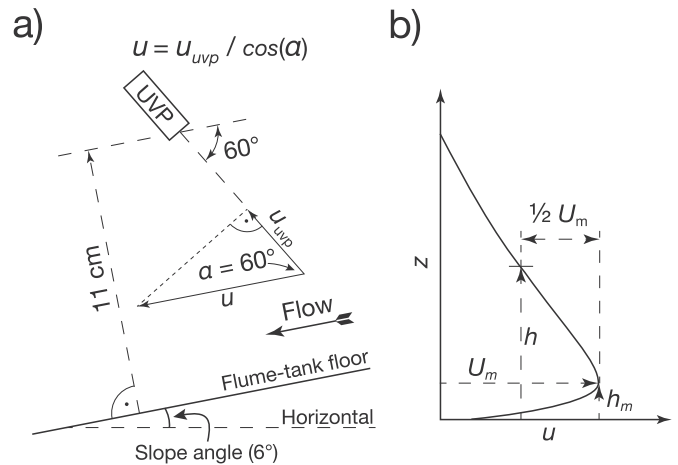

Fig. 4. (a) The orientation of the UVP and the trigonometric calculation to calculate bed-parallel velocities u. The velocity component directed toward the UVP is u_{uvp}. Not to scale. (b) Sketch of a time-averaged velocity profile illustrating the parameterization of the velocity structure.

this averaging window was set to 10 s after the current head passed the measurement location. The duration of the time averaging was 80 s (which was 10 s before the end of the experiment). Fig. 4b illustrates the parameterization of the time-averaged velocity profile, where the vertical axis (z) describes the distance normal to the bed and the horizontal axis (u) the bed-parallel velocity component. The velocity maximum of the flow is U_m and the height of the velocity maximum is h_m.

Flow density was measured by siphoning. Siphon samples were collected 2.5 m downstream of the inlet (i.e. 0.2 m downstream of the UVP), at four different elevations above the flume-tank floor (1, 2, 4, and 8 cm; Fig. 1). The siphon-tube diameter was 7 mm and the average flow velocity in the tube was set to approximately 1 m/s, similar to the velocity scale of the turbidity current. Siphoning commenced ~10 s after the turbidity current head passed the siphon tubes, and was continued until 2 l of mixture was sampled. The volume and weight of each siphon-tube sample were measured, and sediment concentration was calculated from the bulk density of the sample and the specific densities
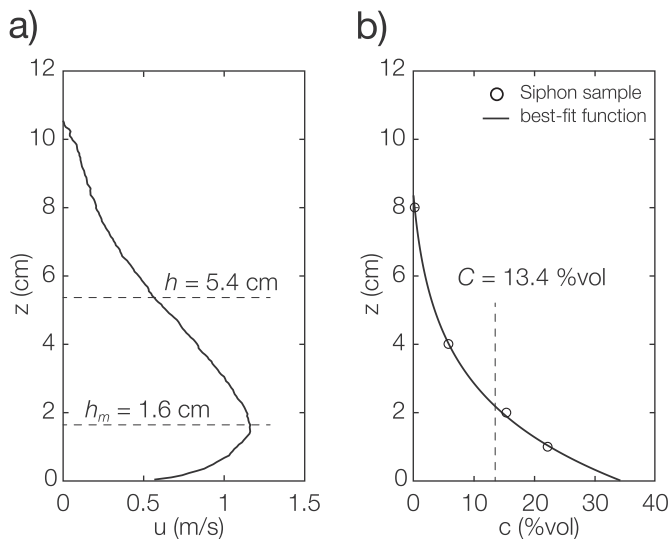
Fig. 5. (a) Time-averaged velocity profile and, (b) sediment concentration profile of the turbidity current in the reference-experiment.

of the water and sediment. A concentration profile was calculated from the best fit of a three-parameter exponential function through the four concentration measurement points, which is defined as:

$$c(z) = e^{\frac{(z-l_1)}{-l_2}} - l_3,\qquad(7)$$

where the sediment concentration at height z is represented by $c(z)$; l_1, l_2, and l_3 are empiric parameters for the curve fitting.

3. Results

3.1. Flow dynamics and confirmation of scaling

The time-averaged velocity profile of the turbidity current in the reference experiment obtained by the UVP is shown in Fig. 5a. The velocity maximum (U_m) was 1.15 m/s, the flow thickens 0.06 m and the depth-average velocity was 0.93 m/s (Table 1). The vertical sediment concentration profile shows stratification with decreasing concentration upwards (Fig. 5b). The depth-average sediment concentration was 13.4% vol, resulting in a depth-average flow density of ~1,11 kg/m³. Shear velocity was calculated with Eq. (4) as 0.07 m/s. These parameters allow to calculate Re_p with 7.2 (Eq. (1)), and θ with 2.9 (Eq. (2)). Both scaling parameters in the reference experiment are within the range of values required for the Shields scaling. (i.e. Re_p of 2–20, and θ of 0.2–10). Depth-average densiometric Froude number was calculated at 2.3, suggesting supercritical flow conditions.

Table 1
Parameters in the reference experiment.

Parameter	Unit	Value
Upper slope	(°)	6
Lower slope	(°)	6
Slope break	(°)	0
Flow thickness h	(m)	0.0536
Height of the maximum velocity h_m	(m)	0.0164
Depth-averaged velocity U	(m/s)	0.9277
Maximum velocity U_m	(m/s)	1.1536
Depth-averaged sediment concentration C	(%vol)	13.3775
Depth-averaged flow density C	kg/m³	1111.7
Froude number Fr'	–	2.2869
Shear velocity u^*	(m/s)	0.0693
Shields parameter θ	–	2.9146
Reynolds particle number Re_p	–	7.1616

3.2. Depositional patterns

Variations in the steepness of the upper and lower slope resulted in a variety of different depositional behaviors, ranging from high rates of deposition to bypass. If deposition occurred, the deposits increased in thickness in a downstream direction, away from the upslope pinch-out.

3.2.1. Upslope pinch-out

The location of the upslope pinch-out was controlled by the steepness of the upper slope. Steepening of the upper slope resulted in the upslope pinch-out moving downdip (Fig. 6a and c). Analysis of all experiments with depositional flows revealed that with an upper slope angle of 5° or less, the upslope pinch-out was located updip of the slope break. If, however, the steepness of the upper slope was 6° or higher, the upslope pinch-out was located on the lower slope, and deposits were detached from the upper slope. A variation in steepness of the lower slope caused no shift of the location of the upslope pinch-out (Fig. 6b and d).

3.2.2. Deposit-thickness-increase

Variation in the steepness of the upper slope resulted in a minor signal in the deposit-thickness-increase (Fig. 7a and c). In contrast, a variation in the steepness of the lower slope had a significant effect on the deposit-thickness-increase, where steepening of the lower slope generally resulted in a decreased deposit-thickness-increase (Fig. 7b and d).

3.2.3. Experiments with a horizontal lower slope

Six experiments were conducted using a horizontal lower slope downstream of the slope break, resulting in rapid deposition downstream of the slope break. These deposits formed an adverse topographic gradient and the turbidity current had to travel upslope, resulting in a significant deceleration. In four of such experiments with an upper slope between 2 and 8°, videos revealed the formation of a roller structure during the last ~10 to 20 s of the experiments (Fig. 8a and Supplementary material Video S1). The roller structure was initiated at the thickest point of the accreted sediment, 3.1 m downstream of the inlet box, and propagated in an upstream direction. The roller structure was characterized by bed-normal oriented velocities, resulting in an abrupt increase in flow thickness (Fig. 8a and Supplementary material Video S1). Deposition rates downstream of the roller structure increased significantly, which resulted in a distinct depositional pattern for these four experiments (Fig. 6c and Supplementary material Fig. S2). The remaining two out of the six experiments that showed rapid deposition downstream of the slope break, also involved a horizontal lower slope but steeper upper slopes (i.e. 10 and 12°). In these experiments no roller structure emerged. Yet toward the end of these two experiments, when the flow waned, some of the deposited sediment remobilized and moved opposite to the original flow direction. This remobilized sediment overprinted the original deposition pattern (Fig. 6c and Supplementary material Fig. S2). In other experiments, on steeper lower slopes and with less depositional flows, no roller structure or sediment mobilization occurred (Fig. 8b and Supplementary material Video S2).

4. Discussion

4.1. Control mechanisms on the upslope pinch-out and the deposit-thickness-increase

The main research objective of this study is to examine how the location of the upslope pinch-out and the deposit-thickness-increase in a slope-break system are controlled by the system's geometry. Geometric parameters in a slope-break system are the steepness of the upper and the lower slopes, and the resulting slope-break angle in between them.
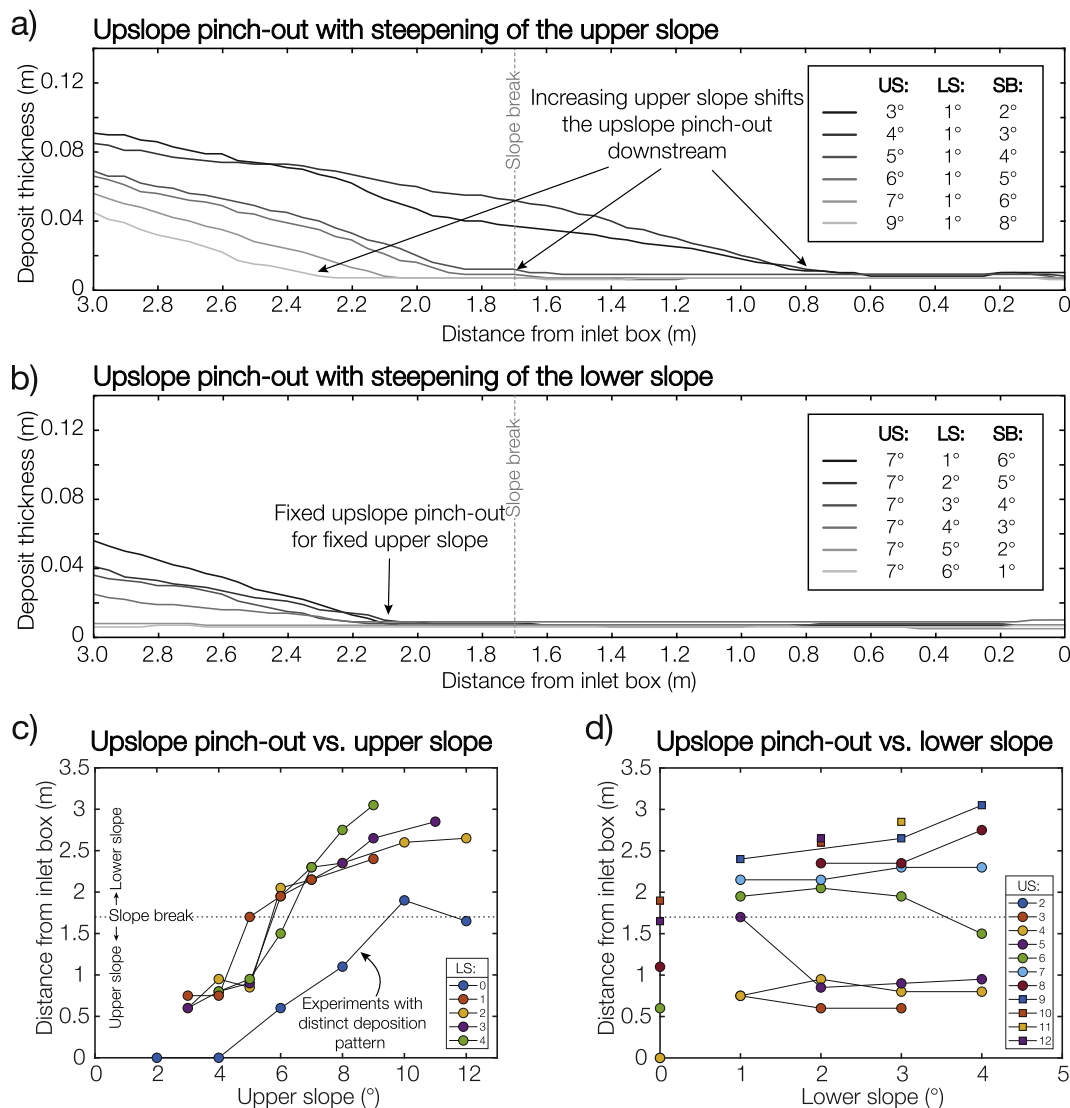
Fig. 6. (a) Deposition profiles of representative experiments, where only the upper slope was varied, and (b), where only the lower slope was varied (cf. Fig. 2). The profiles were measured along the length of the flume tank and flow direction was from right to left. The slope break was at 1.7 m downstream from the inlet box. (c) The location of the upslope pinch-out of all deposition experiments against the steepness of the upper slope, and (d) against the steepness of the lower slope. US: Upper slope, LS: Lower slope, SB: Slope break. Deposition profiles of all experiments are shown in the Supplementary material Fig. S2.

The steepness of the upper slope is the primary control on the up-slope pinch-out; steeper upper slopes force the upslope pinch-out farther downdip (Figs. 6c and 9a). In the experiments, slope-break systems with upper slopes equal or steeper than 6° resulted in upper-slope-detached deposition (Fig. 6c). A slope of 6° was also the most gently dipping slope angle at which flows were still bypassing, suggesting that bypass conditions on the upper slope can be used as a predictor of upper-slope-detached sedimentation patterns. In slope-break systems with an upper-slope gradient too low to achieve bypass conditions, the deposits may onlap onto the upper slope due to the reduction in the turbidity current's transport potential. The downstream shift in upslope pinch-out can be explained with the faster flow velocities on steeper incoming slopes as also suggested Mulder and Alexander (2001). The correlation of the upslope pinch-out with the geometry of the slope-break system was proposed in earlier studies (e.g. Mutti 1985; Wynn et al. 2002) but has not been demonstrated or quantified by previous experimental results.

The upslope pinch-out is also controlled by the transport efficiency of the flow (Mutti 1992). The flow efficiency is controlled by the grain-size distribution of the suspended sediment, the flow volume, and the

flow density (Al Ja'Aidi et al. 2004; Mutti 1992). Large, finer grained flows with a high density are more efficient than smaller, coarser grained flows with a low density (Al Ja'Aidi et al. 2004; Mutti 1992). Highly efficient flows transport their sediment load further into the basin before deposition, and hence, the upslope pinch-out is further downstream. Conversely, the upslope pinch-out produced by a low-efficiency flow will be located further upstream.

In contrast to the upslope pinch-out, which is governed by the upper slope and therefore results from upstream controls, the deposit-thickness-increase is dictated by the lower-slope gradient in a slope-break system. A steeper dipping lower slope resulted in a lower deposit-thickness-increase and, consequently, thinner deposits on the lower slope in the experimental setup (Figs. 7d and 9b). On a gentler dipping lower slope, the flow has less sediment transport capability resulting in a higher deposit-thickness-increase, and thus, thicker deposits in the experiments.

The slope-break angle (i.e. the severity or steepness of the slope break) is an inadequate parameter to describe the system's geometry, since it can represent a variety of different upper and lower slope combinations (cf. Fig.2). Our results indicate that the slope-break angle,
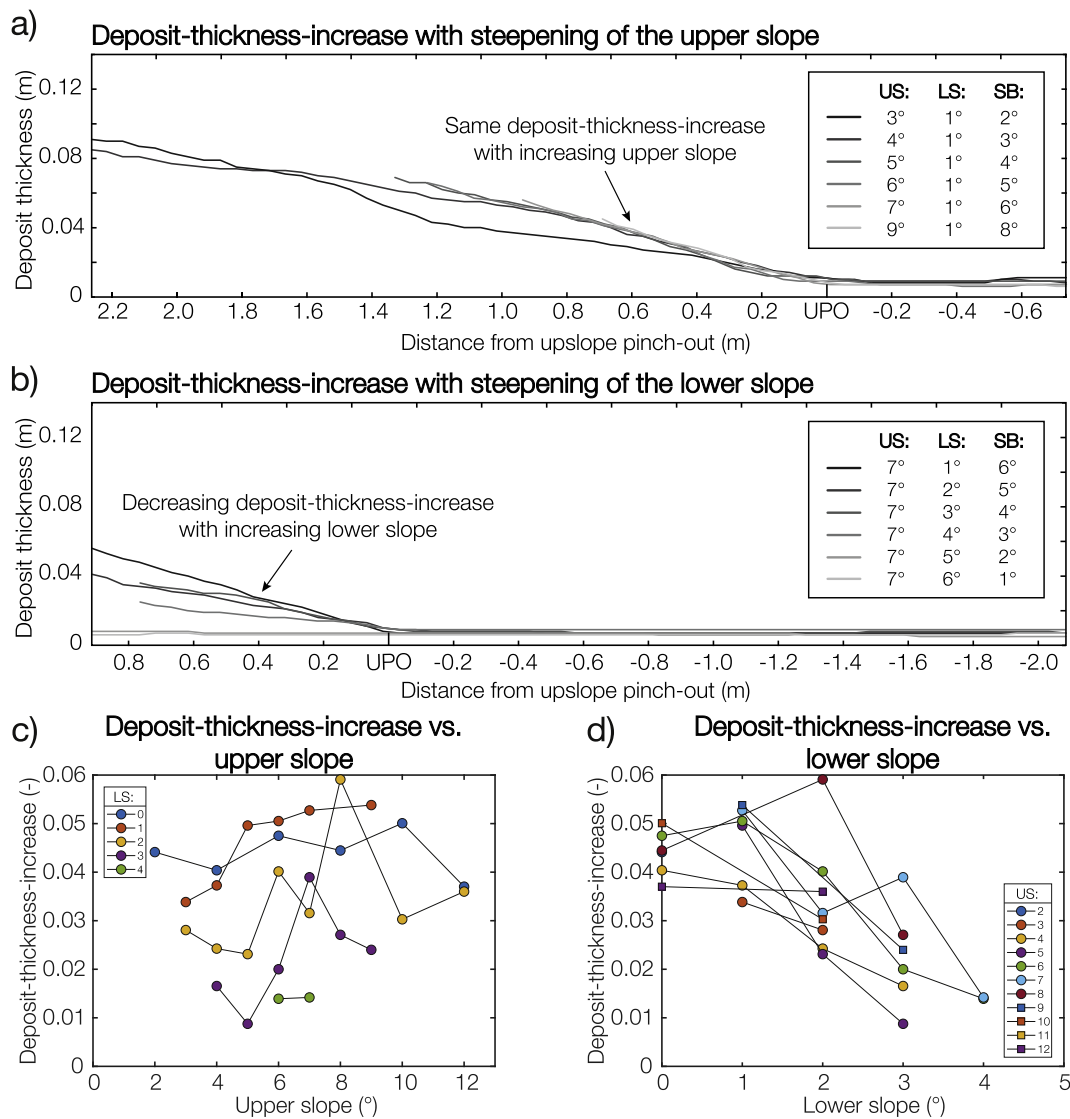
Fig. 7. (a) Deposition profiles of representative experiments, where only the upper slope was varied, and (b), where only the lower slope was varied (cf. Fig. 2). The deposit profiles were aligned with respect to the location of the upslope pinch-out, which was done by a shift of individual profiles along the horizontal axis. (c) The deposit-thickness-increase of all deposition experiments against the steepness of the upper slope, and (d) against the steepness of the lower slope. US: upper slope, LS: lower slope, SB: slope break, UPO: upslope pinch-out. Deposition profiles of all experiments are shown in the Supplementary material Fig. S2.

as a parameter, has no discernable impact on the depositional pattern. This may challenge the interpretations of previous studies, where variations in flow dynamics and deposition patterns are associated with the slope-break angle (e.g. Gray et al. 2005; Mulder and Alexander 2001). In these studies, the increased slope-break angle was achieved by steepening of the upper slope, while the lower slope was kept horizontal. Hence, observed variations in flow dynamics and deposition patterns are likely to be caused by variations of the upper slope, rather than varying the slope-break angle.

In our experiments, slope-break settings with a horizontal lower slope represent a geometrical arrangement that results in a distinct deposition pattern, related to high sedimentation rates on the lower horizontal slope (cf. Fig. 6c). A horizontal lower slope was also used in most previous experiments involving a slope break (Garcia and Parker 1989; Garcia, 1993, 1994; Gray et al., 2005, 2006; Islam and Imran 2010; Mulder and Alexander 2001). Our results suggest that slope-break systems with a horizontal lower slope represent an exceptional condition since it is the only geometrical arrangement where gravitational forces lack a downflow component, or are in fact even reversed with respect to the flow direction due to the development of adverse

gradients. These systems need to be assessed separately.

The present study has considered the effects of a slope break on the depositional signal of turbidity currents. It is important to note that a slope break can be accompanied by a loss of lateral confinement if turbidity currents on the upper slope produce a channel by either erosion, or by buildup of levees, or both, which would create an overprint of the depositional pattern reported here (e.g. Alexander et al. 2008; Pohl et al. 2019; Stacey et al. 2018). Future studies are required to assess the relative contribution of these two factors in the depositional record.

4.2. Implications for natural slope-break systems

4.2.1. Stratigraphic development of slope-break systems

Above-grade slope systems (sensu Prather 2000) may have long-itudinal profiles with multiple slope breaks that create loci of deposition on the slope. There are two types of above-grade slope systems: stepped slopes, characterized by a low relief and terraced topography, and ponded slopes, characterized by enclosed intra-slope basins (Prather et al. 2017). Here we discuss how our results can be used to
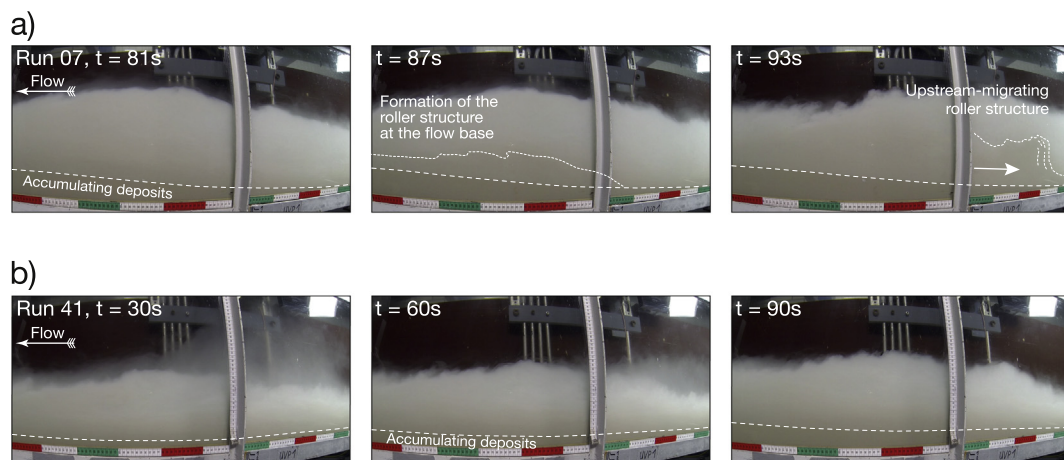
Fig. 8. Snapshots of videos from the turbidity currents through the glass side-wall of the flume tank; see Fig. 1 for field of view. (a) An experiment in which a roller structure emerged on the deposits and migrated upstream. In the experiment, the upper slope was 8° and the lower slope was horizontal. (b) A typical experiment in which sediment was deposited, but no roller structure emerged. In this experiment, the upper slope was 6° and the lower slope was 1°. The green, red, and white scale bars are each 0.1 m long. The videos can be found in the Supplementary material.
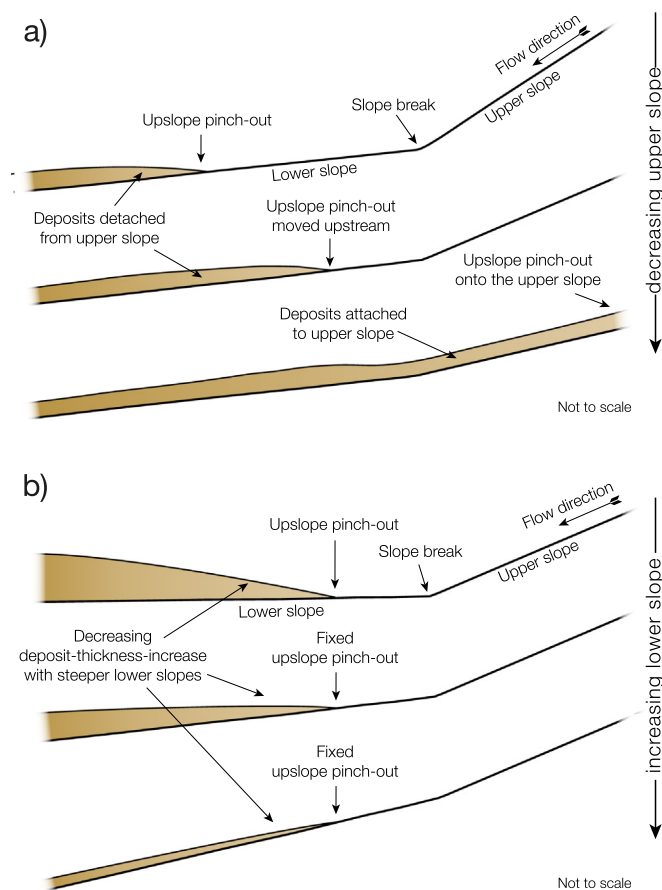
Fig. 9. Sketch illustrating the impact of the upper and lower slopes on the deposition pattern in a slope-break system. (a) Upstream shift of the upslope pinch-out due to the decrease of the upper slope. (b) Decrease of the deposit-thickness-increase due to the increase of the lower slope.

interpret the stratigraphic patterns in terms of the depositional patterns of the turbidites. For this we use as an example a system with a slope-detached sedimentation pattern, the Niger Delta slope, and for a slope-attached sedimentation pattern the Brazos-Trinity Turbidite System in the Gulf of Mexico.

The Niger Delta slope is an above-grade slope system with a stepped

slope topography (Adeogba et al. 2005; Beaubouef and Friedmann 2000; Jobe et al. 2017; Prather et al., 2012a). Each step represents a slope break and forms a small basin. These basins are filled with perched submarine aprons, that have the effect of healing the slope profile and reduce the step morphology over time. The perched submarine apron (OML 134) is subdivided into a lower apron and an overlying upper apron (Prather et al., 2012a) (Fig. 10a). At the basin entry point, which corresponds to the slope break, the lower apron is characterized by multiple erosion features. These erosion features suggest a slope-detached depositional style for the lower apron. In contrast to the erosional features observed in the lower apron, the upper apron is perched over the sediments of the lower apron (Prather et al., 2012a). Hence, there was a switch of the flow behavior from erosion to deposition at the basin point, which implies an up-slope shift of the up-slope pinch-out. This shift may have been due to changes in the geometry of the slope-break system due to tectonic activity, or as the basin was filled with sediment. A up-slope shift of the upslope pinch-out was also described between Fan 3 and 4 in the Tanqua depocenter, Karoo Basin, South Africa (Hansen et al. 2019). The shift between Fan 3 and 4 was interpreted to be caused by a subtle change in slope gradient, which was probably the consequence of the infilling and healing of previous topographic lows and the slope break (Hansen et al. 2019). In addition, externally imposed forces on slope-break systems like flow thickness and delivered grain size will affect its stratigraphic evolution. These external forces might be caused by a transition to less efficient flows with the falling limb of a sediment supply cycle (e.g. Hodgson et al., 2006, 2016), as for example described for the evolution of channel systems (Jobe et al. 2015).

The Brazos-Trinity Turbidite System, offshore the Gulf of Mexico, is an above-grade ponded-slope system (Badalini et al. 2000; Prather et al., 1998, 2012b, 2017; Winker 1996). The Brazos-Trinity Turbidite System consists of four intra-slope basins, connected by a channel system (Prather et al., 2012b). The proximal region of each ponded basin is characterized by a slope break, affecting the basin's sedimentation style. A seismic section through Brazos-Trinity Basin II reveals a succession of perched aprons onlapping onto the upstream slope (Fig. 10b). This infilling pattern differs from that of the Niger Delta slope, in that it shows no erosion at the basin entry point (Prather et al., 2012a). Hence, the slope of the incoming channel of Brazos-Trinity Basin II is not steep enough to maintain bypass conditions for the turbidity currents on that slope. This results in the slope-attached onlap pattern of the perched aprons in the Brazos-Trinity Basin II, and is consistent with the experimental observations.
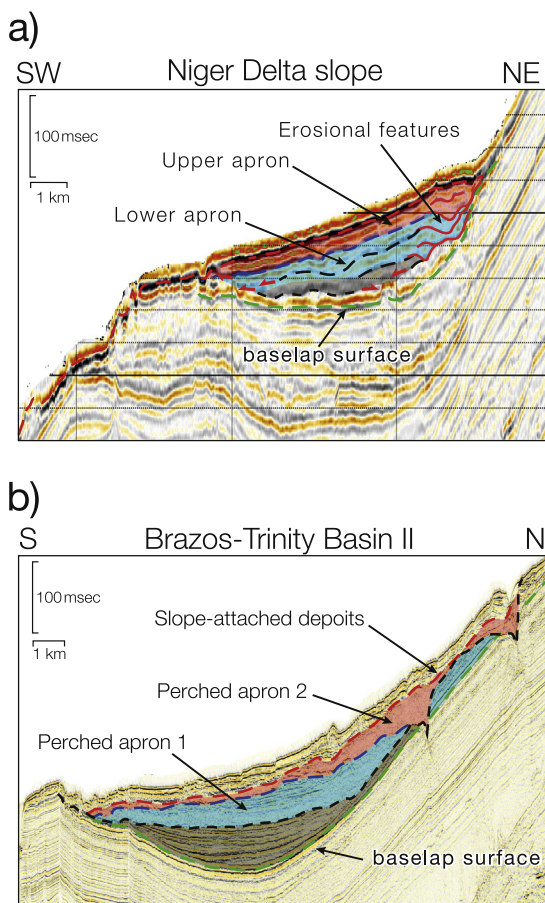
Fig. 10. (a) Seismic longitudinal-section of the Niger Delta slope, an example of a slope-detached sedimentation pattern. The red lines indicate erosive contacts at the slope break (i.e. the basin entry point). Modified after: Prather et al. (2012a). (b) Seismic longitudinal-section of the Brazos-Trinity Basin II, an example of slope-attached sedimentation with less scour development and an onlapping sedimentation pattern. Modified after: Prather et al. (2012b). (For interpretation of the references to colour in this figure legend, the reader is referred to the web version of this article.)

4.2.2. Plunge pools

Plunge pools represent an end member slope-break system and usually form in geometric arrangements with a steep upper slope and a high slope-break angle (Bourget et al. 2011; Lee et al. 2002). Lee et al. (2002) suggested an abrupt slope break of > 4° as the minimum criterion for the formation of a plunge pool, although observations suggest that plunge pools are well developed at slope breaks of > 15°. The continental slope of the California Margin, for example, is ~20° steep and characterized by a series of gullies that terminate in plunge pools (Lee et al. 2002); similar slope angles have been reported along the Makran system (Bourget et al. 2011).

Lee et al. (2002) describe in their hydraulic-jump-pool process-model a hydraulic jump which emerged at the slope break due to the sharp decrease in slope. Rapid deposition downstream of the hydraulic jump forms a constructional rampart and in consequence a plunge pool. In case of our experiments, the above-mentioned scenario would correspond to slope-break settings using a steep upper slope and a horizontal lower slope, which resulted in high sedimentation rates downstream of the slope break. The deposits on the lower horizontal slope formed an adverse slope, comparable to the constructional rampart of a plunge pool. In the experiments, this adverse slope resulted in the emergence of an upstream migrating roller structure (Fig. 8a), which is likely to represent a hydraulic jump (e.g. Komar 1971; Vellinga et al. 2018). The results of our experiments therefore suggest that the

hydraulic jump in a submarine plunge pool can also result from the deposition of the rampart, initiating after the formation of the plunge pool, rather than as an initial effect of the slope break. Thus, the initial formation of a constructional rampart can also be explained with high sedimentation rates downstream of the slope break rather than with the formation of a hydraulic jump.

4.2.3. The formation of upslope stratigraphic traps

The steepness of the upper slope in slope-break systems provides an additional tool for the estimation of potential hydrocarbon reservoirs. If sandy deposits downstream of a slope break are connected to the upslope slope sands, potential hydrocarbon reserves may migrate through these sands out off the main reservoir. Such thin connected slope sands are therefore known as thief sands in reservoir evaluation. In contrast, a system with slope-detached sand sedimentation may result in the formation of upslope stratigraphic traps and sealed reservoirs (Amy 2019; Doré and Robbins 2005; Ray et al. 2010). This type of stratigraphic trap was termed a bypass-related pinchout trap by Amy (2019). Thief sands can be thin (e.g. Brooks et al. 2018; Hansen et al. 2019), and therefore poorly imaged on seismic data, which means that the presence of a bypass-related trap can be one of the main risks that is under debate in subsurface exploration. In such cases, it can be useful to apply learnings from studies on the control of depositional patterns on attached/detached sedimentation. The results of the experiments indicate that the steepness to the upper slope adjacent to the slope break controls whether or not deposits drape onto the slope. If the upper slope is steep enough to maintain bypass conditions, deposits are likely to be detached from the upper slope. In such a slope-break setting, the formation of an upslope stratigraphic trap is more likely. Conversely, upper slopes that are not steep enough to maintain bypass conditions are more likely to form attached deposits, and therefore poorly sealed reservoirs. Already subtle changes in slope gradients can result in a shift of the upslope pinch-out as implied by field relations in the Tanqua depocenter, Karoo Basin, with significant implications for the risk assessment of stratigraphic traps (Hansen et al. 2019). Our findings simplify the sedimentological risk assessment for stratigraphic traps, because the basin floor steepness and the slope-break angle can be disregarded as primary controls on thief sands. As discussed above, considerations of the steepness of the incoming slope must always be combined with considerations of flow scales and efficiency. We therefor echo the conclusion of Amy (2019) that future work improving stratigraphic trap evaluation should try to quantify the critical slope needed to maintain bypass conditions in turbidity currents.

5. Conclusions

The Shields-scaled experiments of the present study mimic the transition from a bypassing to a depositional turbidity current in a slope-break system. Furthermore, we present the first experiments involving dipping lower slopes, downstream of the slope break, as well as testing a variety of 45 different combinations of the upper and lower slopes.

1) The geometric control parameters in a high-density turbidity current slope-break system are the steepness of the upper and lower slope. Our results show that the resulting slope-break angle between these two slopes, as a parameter, has no clearly discernible impact on the deposition pattern, since it represents a variety of different upper and lower slope combinations. Therefore, we suggest that in a slope-break system, it is not the slope-break angle which should be considered as the main parameter or driving factor in this system, but rather the combination of the incoming upper and outgoing lower slopes.

2) In our experiments slope-break systems with a horizontal lower slope resulted in high sedimentation rates on the horizontal lower slope and the formation of a roller structure, producing a distinctly

different deposition pattern from experiments with an inclined lower slope. Furthermore, gravitational forces lack a downflow component on a horizontal lower slope. Slope-break systems with a horizontal lower slope represent an exceptional condition and should, therefore, be considered separately from slope-break systems with dipping lower slopes.

3) In a slope-break system the location of the upslope pinch-out is controlled by the upper slope, whereas the value of the deposit-thickness-increase is controlled by the lower slope. An increase in the steepness of the upper slope shifts the upslope pinch-out basinwards, making a connection between basin floor sediments and slope sediments less likely. Increasing the angle of the lower slope results in thinner deposits in the experimental set-up, but has no impact on the location of the upslope pinch-out.

4) The steepness of the upper slope may be useful to estimate the potential for hydrocarbon traps in slope-break systems. Upper slopes steep enough to maintain bypass condition result in a slope-detached sedimentation pattern, and an increased likelihood of the formation of an upslope stratigraphic trap. Whereas upper slopes not steep enough to maintain bypass conditions result in a slope-attached sedimentation and the formation of thief sands.

Declaration of competing interest

The authors declare that they have no known competing financial interests or personal relationships that could have appeared to influence the work reported in this paper.

Acknowledgments

Appendix A. Supplementary data

Supplementary data to this article can be found online at https://doi.org/10.1016/j.margeo.2020.106160.

References

Adeogba, A.A., McHargue, T.R., Graham, S.A., 2005. Transient fan architecture and depositional controls from near-surface 3-D seismic data, Niger Delta continental slope. Am. Assoc. Pet. Geol. Bull. 89, 627–643. https://doi.org/10.1306/11200404025.

Al Ja'Aidi, O.S., McCaffrey, W.D., Kneller, B.C., 2004. Factors influencing the deposit geometry of experimental turbidity currents: implications for sand-body architecture in confined basins. Geol. Soc. London. Spec. Publ. 222, 45–58. https://doi.org/10.1144/GSL.SP.2004.222.01.04.

Alexander, J., McLelland, S.J., Gray, T.E., Vincent, C.E., Leeder, M.R., Ellett, S., 2008. Laboratory sustained turbidity currents form elongate ridges at channel mouths. Sedimentology 55, 845–868. https://doi.org/10.1111/j.1365-3091.2007.00923.x.

Amy, L.A., 2019. A review of producing fields inferred to have upslope stratigraphically trapped turbidite reservoirs: trapping styles (pure and combined), pinchout formation and depositional setting. Am. Assoc. Pet. Geol. Bull. https://doi.org/10.1306/02251917408.

Amy, L., Kneller, B., McCaffrey, W., 2000. Evaluating the links between turbidite characteristics and gross system architecture: upscaling insights from the turbidite sheet-system of Peïra Cava, SE France, in: Deep-water Reservoirs of the World: 20th Annual. Society of Economic Paleontologists and Mineralogists, pp. 1–15. doi:https://doi.org/10.5724/gcs.00.15.0001.

Azpiroz-Zabala, M., Cartigny, M.J.B., Talling, P.J., Parsons, D.R., Sumner, E.J., Clare, M.A., Simmons, S.M., Cooper, C., Pope, E.L., 2017. Newly recognized turbidity current structure can explain prolonged flushing of submarine canyons. Sci. Adv. 3, 1–12. https://doi.org/10.1126/sciadv.1700200.

Badalini, G., Kneller, B., Winker, C.D., 2000. Architecture and process in the Late Pleistocene Trinity–Brazos turbidite system, Gulf of Mexico, in: Weimer, P., Slatt, R. M., Coleman, J., Rosen, N.C., Nelson, H., Bouma, A.H., Styzen, M.J., Lawrence, D.T. (Eds.), Deep-water Reservoirs of the World: Gulf Coast Section. SEPM Foundation, 20th Annual Bob F. Perkins Research Conference, pp. 16–34.

Beaubouef, R.T., Friedmann, S.J., 2000. High resolution seismic/sequence stratigraphic framework for the evolution of Pleistocene intra slope basins, Western Gulf of Mexico: depositional models and reservoir analogs. Deep. Reserv. World 20th Annu. Conf. 40–60. doi:https://doi.org/10.5724/gcs.00.15.0040.

Bourget, J., Zaragosi, S., Ellouz-Zimmermann, N., Mouchot, N., Garlan, T., Schneider, J.L., Lanfumey, V., Lallemant, S., 2011. Turbidite system architecture and sedimentary processes along topographically complex slopes: the Makran convergent margin. Sedimentology 58, 376–406. https://doi.org/10.1111/j.1365-3091.2010.01168.x.

Boyer, F., Guazzelli, É., Pouliquen, O., 2011. Unifying suspension and granular rheology. Phys. Rev. Lett. 107, 1–5. https://doi.org/10.1103/PhysRevLett.107.188301.

Brooks, H.L., Hodgson, D.M., Brunt, R.L., Peakall, J., Hofstra, M., Flint, S.S., 2018. Deep-water channel-lobe transition zone dynamics: processes and depositional architecture, an example from the Karoo Basin. South Africa. GSA Bull. 130, 1723–1746. https://doi.org/10.1130/B31714.1.

Buckee, C., Kneller, C., Peakall, J., 2001. Turbulence structure in steady, solute-driven gravity currents, in: Mccaffrey, W.D., Kneller, B., Peakall, Jeff (Eds.), Particulate Gravity Currents. International Association of Sedimentologists, Special Publication 31, Blackwell Science, pp. 173–188.

Cartigny, M.J.B., Eggenhuisen, J.T., Hansen, E.W.M., Postma, G., 2013. Concentration-dependent flow stratification in experimental high-density turbidity currents and their relevance to turbidite facies models. J. Sediment. Res. 83, 1046–1064. https://doi.org/10.2110/jsr.2013.71.

Daly, R.A., 1936. Origin of submarine "canyons." Am. J. Sci. 31, 401–420. doi:https://doi.org/10.2475/ajs.s5-31.186.401.

de Leeuw, J., Eggenhuisen, J.T., Cartigny, M.J.B., 2016. Morphodynamics of submarine channel inception revealed by new experimental approach. Nat. Commun. 7, 1–7. https://doi.org/10.1038/ncomms10886.

de Leeuw, J., Eggenhuisen, J.T., Cartigny, M.J.B., 2018a. Linking submarine channel–levee facies and architecture to flow structure of turbidity currents: insights from flume tank experiments. Sedimentology 65, 931–951. https://doi.org/10.1111/sed.12411.

de Leeuw, J., Eggenhuisen, J.T., Spychala, Y.T., Heijnen, M.S., Pohl, F., Cartigny, M.J.B., 2018b. Sediment volume and grain-size partitioning between submarine channel–levee systems and lobes: an experimental study. J. Sediment. Res. 88, 777–794. https://doi.org/10.1016/j.rbmo.2014.07.005.

Doré, G., Robbins, J., 2005. The Buzzard field, in: Doré, A., Vining, B.A. (Eds.), Petroleum Geology: North-West European Global Perspectives - Proceedings of the 6th Petroleum Geology Conference. pp. 241–252.

Eggenhuisen, J.T., Cartigny, M.J.B., de Leeuw, J., 2017. Physical theory for near-bed turbulent particle suspension capacity. Earth Surf. Dyn. 5, 269–281. https://doi.org/10.5194/esurf-5-269-2017.

Eggenhuisen, J.T., Tilston, M.C., de Leeuw, J., Pohl, F., Cartigny, M.J.B., 2019. Turbulent diffusion modelling of sediment in turbidity currents; an experimental validation of the Rouse approach. Depos. Rec. 1–14. https://doi.org/10.1002/dep2.86.

Ferguson, R.A., Kane, I.A., Eggenhuisen, J.T., Pohl, F., Tilston, M., Yvonne, T., 2020. Entangled external and internal controls on submarine fan evolution: an experimental perspective. EarthArXiv 1–38.

Fernandes, A.M., Buttles, J., Mohrig, D., 2019. Flow-substrate interactions in aggrading and degrading submarine channels. EarthArXiv. doi:10.31223/osf.io/ceyhk.

Garcia, M.H., 1993. Hydraulic jumps in sediment-driven bottom currents. J. Hydraul. Eng. 119, 1094–1117. https://doi.org/10.1061/(ASCE)0733-9429(1993)119:10(1094).

Garcia, M.H., 1994. Depositional turbidity currents laden with poorly sorted sediment. J. Hydraul. Eng. 120, 1240–1263. https://doi.org/10.1061/(ASCE)0733-9429(1994)120:11(1240).

Garcia, M., Parker, G., 1989. Experiments on hydraulic jumps in turbidity currents near a canyon-fan transition. Science (80-.). 245, 393–396. doi:https://doi.org/10.1126/science.245.4916.393.

Gray, T.E., Alexander, J., Leeder, M.R., 2005. Quantifying velocity and turbulence structure in depositing sustained turbidity currents across breaks in slope. Sedimentology 52, 467–488. https://doi.org/10.1111/j.1365-3091.2005.00705.x.

Gray, T.E., Alexander, J., Leeder, M.R., 2006. Longitudinal flow evolution and turbulence structure of dynamically similar, sustained, saline density and turbidity currents. J. Geophys. Res. Ocean. 111, 1–14. doi:https://doi.org/10.1029/2005JC003089.

Hansen, L.A.S., Hodgson, D.M., Pontén, A., Bell, D., Flint, S., 2019. Quantification of Basin-floor Fan Pinchouts: Examples From the Karoo Basin. South Africa 7, 1–20. https://doi.org/10.3389/feart.2019.00012.

Hodgson, D.M., Flint, S.S., Hodgetts, D., Drinkwater, N.J., Johannessen, E.P., Luthi, S.M., 2006. Stratigraphic evolution of fine-grained submarine fan systems, Tanqua Depocenter, Karoo Basin, South Africa. J. Sediment. Res. 76, 20–40. https://doi.org/10.2110/jsr.2006.03.

Hodgson, D.M., Kane, I.A., Flint, S.S., Brunt, R.L., Ortiz-Karpf, A., 2016. Time-transgressive confinement on the slope and the progradation of basin-floor fans: implications for the sequence stratigraphy of deep-water deposits. J. Sediment. Res. 86, 73–86. https://doi.org/10.2110/jsr.2016.3.

Heerema, C.J., Talling, P.J., Cartigny, M.J., Paull, C.K., Bailey, L., Simmons, S.M., Parsons, D.R., Clare, M.A., Gwiazda, R., Lundsten, E., Anderson, K., Maier, K.L., Xu, J.P., Sumner, E.J., Rosenberger, K., Gales, J., Mcgann, M., Carter, L., Pope, E., Coordinated, M., Experiment, C., Team, C.C.E., 2020. What determines the downstream evolution of turbidity currents? Earth Planet. Sci. Lett. 532, 116023. https://doi.org/10.1016/j.epsl.2019.116023.

Hughes, S.A., 1993. Physical Models and Laboratory Techniques in Coastal Engineering. World Scientific.

Islam, M.A., Imran, J., 2010. Vertical structure of continuous release saline and turbidity currents. J. Geophys. Res. Ocean. 115, 1–14. https://doi.org/10.1029/2009JC005365.

Jobe, Z.R., Sylvester, Z., Parker, A.O., Howes, N., Slowey, N., Pirmez, C., 2015. Rapid adjustment of submarine channel architecture to changes in sediment supply. J. Sediment. Res. 85, 729–753. https://doi.org/10.2110/jsr.2015.30.

Jobe, Z.R., Sylvester, Z., Howes, N., Pirmez, C., Parker, A., Cantelli, A., Smith, R., Wolinsky, M.A., O'Byrne, C., Slowey, N., Prather, B., 2017. High-resolution, millennial-scale patterns of bed compensation on a sand-rich intraslope submarine fan, western Niger Delta slope. Bull. Geol. Soc. Am. 129, 23–37. https://doi.org/10.1130/B31440.1.

Kneller, B.C., Branney, M.J., 1995. Sustained high-density turbidity currents and the deposition of thick massive sands. Sedimentology 42, 607–616. https://doi.org/10.1111/j.1365-3091.1995.tb00395.x.

Komar, P.D., 1971. Hydraulic jumps in turbidity currents. Bull. Geol. Soc. Am. 82, 1477–1488. https://doi.org/10.1130/0016-7606(1971)82[1477:HJITC]2.0.CO;2.

Kuenen, P.H., Migliorini, C.I., 1950. Turbidity currents as a cause of graded bedding. J. Geol. 58, 91–127. https://doi.org/10.1086/625710.

Launder, B.E., Rodi, W., 1983. The turbulent wall jet measurements and modeling. Annu. Rev. Fluid Mech. 15, 429–459. https://doi.org/10.1146/annurev.fl.15.010183.002241.

Lee, S.E., Talling, P.J., Ernst, G.G.J., Hogg, A.J., 2002. Occurrence and origin of submarine plunge pools at the base of the US continental slope. Mar. Geol. 185, 363–377. https://doi.org/10.1016/S0025-3227(01)00298-5.

Maier, K.L., Fildani, A., Paull, C.K., Graham, S.A., McHargue, T.R., Caress, D.W., McGann, M., 2011. The elusive character of discontinuous deep-water channels: new insights from Lucia Chica channel system, offshore California. Geology 39, 327–330. https://doi.org/10.1130/G31589.1.

Marr, J.G., Shanmugam, G., Parker, G., 2001. Experiments on subaqueous sandy gravity flows: the role of clay and water content in flow dynamics and depositional structures. Bull. Geol. Soc. Am. 113, 1377–1386. https://doi.org/10.1130/0016-7606(2001)113<1377:EOSSGF>2.0.CO;2.

Middleton, G. V., Southard, J.B., 1984. Mechanics of Sediment Movement. SEPM, Eastern Section Short Course 3 Providence, 401 pp.

Miramontes, E., Eggenhuisen, J.T., Silva Jacinto, R., Poneti, G., Pohl, F., Normandeau, A., Campbell, D.C., Hernández-Molina, F.J., 2020. Channel-levee evolution in combined contour current–turbidity current flows from flume-tank experiments. Geology XX, 1–5. doi:https://doi.org/10.1130/G47111.1.

Mulder, T., Alexander, J., 2001. Abrupt change in slope causes variation in the deposit thickness of concentrated particle-driven density currents. Mar. Geol. 175, 221–235. https://doi.org/10.1016/S0025-3227(01)00114-1.

Mutti, E., 1985. Turbidite systems and their relations to depositional sequences. In: Zuffa, G.G. (Ed.), Provenance of Arenites: NATO-ASI Series. Reidel, Dordrecht, pp. 65–93.

Mutti, E., 1992. Turbidite Sandstones. Agip, Istituto di geologia, Università di Parma. 275 pp.

Mutti, E., Normark, W.R., 1987. Comparing examples of modern and ancient turbidite systems: problems and concepts. In: Leggett, J.K., Zuffa, G.G. (Eds.), Marine Clastic Sedimentology. Springer, Dordrecht, pp. 1–38. https://doi.org/10.1007/978-94-009-3241-8_1.

Mutti, E., Normark, W.R., 1991. An integrated approach to the study of turbidite systems. In: Weimer, P., Link, M.H. (Eds.), Seismic Facies and Sedimentary Processes of Submarine Fans and Turbidite Systems. Springer, New York, pp. 75–106. https://doi.org/10.1007/978-1-4684-8276-8_4.

Mutti, E., Bernoulli, D., Lucchi, F.R., Tinterri, R., 2009. Turbidites and turbidity currents from alpine "flysch" to the exploration of continental margins. Sedimentology 56, 267–318. https://doi.org/10.1111/j.1365-3091.2008.01019.x.

Paull, C.K., Talling, P.J., Maier, K.L., Parsons, D., Xu, J., Caress, D.W., Gwiazda, R., Lundsten, E.M., Anderson, K., Barry, J.P., Chaffey, M., O'Reilly, T., Rosenberger, K.J., Gales, J.A., Kieft, B., McGann, M., Simmons, S.M., McCann, M., Sumner, E.J., Clare, M.A., Cartigny, M.J., 2018. Powerful turbidity currents driven by dense basal layers. Nat. Commun. 9, 4114. https://doi.org/10.1038/s41467-018-06254-6.

Peakall, J., Ashworth, P., Best, J., 1996. Physical modelling in fluvial geomorphology: principles, applications and unresolved issue. In: Rhoads, B.L., Thorn, C.E. (Eds.), The Scientific Nature of Geomorphology. John Wiley and Sons, Chichester, pp. 221–253.

Pettingill, H.S., 2004. Global overview of deepwater exploration and production, in: Weimer, P. (Ed.), Petroleum Systems of Deepwater Settings. Society of Exploration Geophysicists and European Association of Geoscientists and Engineers, pp. 1–40. doi:https://doi.org/10.1190/1.9781560801955.ch2.

Pohl, F., Eggenhuisen, J.T., Kane, I.A., Clare, M.A., 2020. Transport and burial of microplastics in deep-marine sediments by turbidity currents. Environ. Sci. Technol In press.

Pohl, F., Eggenhuisen, J.T., Tilston, M., Cartigny, M.J.B., 2019. New flow relaxation mechanism explains scour fields at the end of submarine channels. Nat. Commun. 10, 4425. https://doi.org/10.1038/s41467-019-12389-x.

Prather, B.E., 2000. Calibration and visualization of depositional process models for above-grade slopes: a case study from the Gulf of Mexico. Mar. Pet. Geol. 17, 619–638. https://doi.org/10.1016/S0264-8172(00)00015-5.

Prather, B.E., 2003. Controls on reservoir distribution, architecture and stratigraphic trapping in slope settings. Mar. Pet. Geol. 20, 529–545. https://doi.org/10.1016/j.marpetgeo.2003.03.009.

Prather, B.E., Booth, J.R., Steffens, G.S., Craig, P.A., 1998. Succession of seismic facies of intraslope basins, deep-water Gulf of Mexico 1. Am. Assoc. Pet. Geol. Bull. 82, 701–728. https://doi.org/10.1306/1D9BC5D9-172D-11D7-8645000102C1865D.

Prather, B.E., Pirmez, C., Sylvester, Z., Prather, D.S., 2012a. Stratigraphic response to evolving geomorphology in a submarine apron perched on the upper Niger Delta slope, in: Prather, B.E., Deptuck, M.E., Mohrig, D., van Hoorn, B., Wynn, R.B. (Eds.), Application of the Principles of Seismic Geomorphology to Continental-slope and Base-of-slope Systems: Case Studies From Seafloor and Near-seafloor Analogues. SEPM (Society for Sedimentary Geology), Special Publication 99, pp. 145–161. doi:https://doi.org/10.2110/pec.12.99.0145.

Prather, B.E., Pirmez, C., Winker, C.D., 2012b. Stratigraphy of linked intraslope basins: Brazos–Trinity system western Gulf of Mexico, in: Prather, B.E., Deptuck, M.E., Mohrig, D., van Hoorn, B., Wynn, R.B. (Eds.), Application of the Principles of Seismic Geomorphology to Continental-slope and Base-of-slope Systems: Case Studies from Seafloor and Near-seafloor Analogues. SEPM (Society for Sedimentary Geology). Special Publication 99, 83–109. https://doi.org/10.2110/pec.12.99.0083.

Prather, B.E., O'Byrne, C., Pirmez, C., Sylvester, Z., 2017. Sediment partitioning, continental slopes and base-of-slope systems. Basin Res. 29, 394–416. https://doi.org/10.1111/bre.12190.

Prélat, A., Covault, J.A., Hodgson, D.M., Fildani, A., Flint, S.S., 2010. Intrinsic controls on the range of volumes, morphologies, and dimensions of submarine lobes. Sediment. Geol. 232, 66–76. https://doi.org/10.1016/j.sedgeo.2010.09.010.

Ray, F.M., Pinnock, S.J., Katamish, H., Turnbull, J.B., 2010. The Buzzard Field: anatomy of the reservoir from appraisal to production. Pet. Geol. From Matur. Basins to New Front. 7th Pet. Geol. Conf. 369–386. doi:https://doi.org/10.1144/0070369.

Rouse, H., 1937. Modern conceptions of the mechanics of fluid turbulence. Am. Soc. Civ. Eng. Trans. 102, 463–543.

Shields, A., 1936. Anwendung der Aehnlichkeitsmechanig und der Turbulenzforschung auf die Geschiebebewegung. Mitteilungen der Preußischen Versuchsanstalt für Wasserbau und Schiffbau. Technische Hochschule Berlin, 25 pp.

Stacey, C.D., Hill, P.R., Talling, P.J., Enkin, R.J., Hughes Clarke, J., Lintern, D.G., 2018. How turbidity current frequency and character varies down a fjord-delta system: combining direct monitoring, deposits and seismic data. Sedimentology 66, 1–31. https://doi.org/10.1111/sed.12488.

Stevenson, C.J., Jackson, C.A.-L., Hodgson, D.M., Hubbard, S.M., Eggenhuisen, J.T., 2015. Deep-water sediment bypass. J. Sediment. Res. 85, 1058–1081. https://doi.org/10.2110/jsr.2015.63.

Straccia, J.R., Prather, B.E., 1999. Stratigraphic traps in deep-water turbidite reservoirs at the base of depositional slope. SPE 56894.

Talling, P.J., Allin, J., Armitage, D.A., Arnott, R.W., Cartigny, M.J., Clare, M.A., Felletti, F., Covault, J.A., Girardclos, S., Hansen, E., Hill, P.R., Hiscott, R.N., Hogg, A.J., Hughes Clarke, J., Jobe, Z.R., Malgesini, G., Mozzato, A., 2015. Key future directions for research on turbidity currents and their deposits. J. Sediment. Res. 85, 153–169. https://doi.org/10.2110/jsr.2015.03.

Toniolo, H., Parker, G., Voller, V., Beaubouef, R.T., 2006. Depositional turbidity currents in diapiric minibasins on the continental slope: experiments–numerical simulation and upscaling. J. Sediment. Res. 76, 798–818. https://doi.org/10.2110/jsr.2006.072.

van Rijn, L.C., 1993. Principles of sediment transport in rivers, estuaries and coastal seas, Aqua publications. Aqua Publications. 790 pp., Amsterdam. doi:https://doi.org/10.1002/9781444308785.

Vellinga, A.J., Cartigny, M.J.B., Eggenhuisen, J.T., Hansen, E.W.M., 2018. Morphodynamics and depositional signature of low-aggradation cyclic steps: new insights from a depth-resolved numerical model. Sedimentology 65, 540–560. https://doi.org/10.1111/sed.12391.

Weimer, P., Slatt, R., 2004. Hybrid-type deepwater reservoirs and pitfalls in the interpretation of deepwater sandstones. In: Slatt, R.M. (Ed.), Weimer, P. Petroleum Systems of Deepwater Settings, Society of Exploration Geophysicists and European Association of Geoscientists and Engineers, pp. 1–22. https://doi.org/10.1190/1.9781560801955.ch8.

Winker, C.D., 1996. High-resolution seismic stratigraphy of a Late Pleistocene submarine fan ponded by salt-withdrawal mini-basins on the Gulf of Mexico continental slope, in: Offshore Technology Conference. Offshore Technology Conference, pp. 619–628. doi:https://doi.org/10.4043/8024-MS.

Wynn, R.B., Kenyon, N.H., Masson, D.G., Stow, D.A.V., Weaver, P.P.E., 2002. Characterization and recognition of deep-water channel-lobe transition zones. Am. Assoc. Pet. Geol. Bull. 86, 1441–1462. https://doi.org/10.1306/61eedcc4-173e-11d7-8645000102c1865d.

Yalin, S.M., 1971. Theory of Hydraulic Models. (Macmillan International Higher Education).

Zou, C., Zhai, G., Zhang, G.G., Wang, H., Zhang, G.G., Li, J., Wang, Z., Wen, Z., Ma, F., Liang, Y., Yang, Z., Li, X., Liang, K., 2015. Formation, distribution, potential and prediction of global conventional and unconventional hydrocarbon resources. Pet. Explor. Dev. 42, 14–28. https://doi.org/10.1016/S1876-3804(15)60002-7.